


 Cite this: *RSC Adv.*, 2025, 15, 14195

# A highly luminescent 3-phenylfluoranthene-modified $g\text{-C}_3\text{N}_4$ derivative used as a metal-free phosphor in white light-emitting diodes†

 Jinghao Zhang,‡ Long Wang,‡ Huaijun Tang, \* Xiang Li, Aijing Jiang, Yibing Wu,\* Shanglan Xian, Rongman Xia, Yifei Li, Zhouyang Jiang and Zhengliang Wang

 Received 23rd March 2025  
 Accepted 28th April 2025

DOI: 10.1039/d5ra02050f

[rsc.li/rsc-advances](http://rsc.li/rsc-advances)

Here, using melamine as the main precursor and 6-(4-(fluoranthen-3-yl)phenyl)-1,3,5-triazine-2,4-diamine as the dopant, a 3-phenylfluoranthene-modified greenish-yellow-emitting  $g\text{-C}_3\text{N}_4$  derivative was synthesized *via* thermal polymerization. Excited by blue light chips, high-performance white LEDs were fabricated by using the derivative and red-emitting  $\text{K}_2\text{SiF}_6\text{:Mn}^{4+}$  as phosphors.

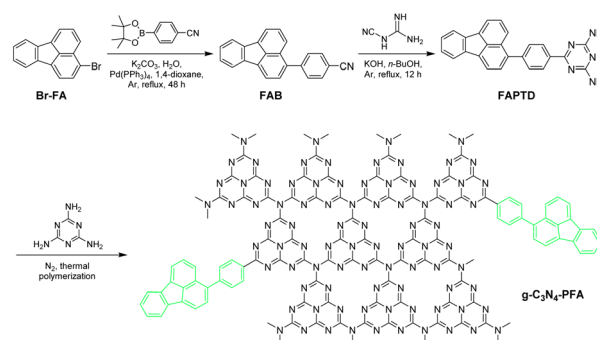
Graphitic carbon nitride ( $g\text{-C}_3\text{N}_4$ ) and its derivatives are a class of metal-free polymeric conjugated semiconductors and two-dimensional (2D) layered materials, which can be easily synthesized *via* thermal polymerization by many cheap, nitrogen-rich and source-abundant precursors, such as melamine, dicyandiamide, urea and thiourea.<sup>1–4</sup> In the past decade or so, they have been extensively studied and applied in multiple fields, such as photocatalysis,<sup>1,2</sup> electrocatalysis,<sup>3</sup> energy storage,<sup>4</sup> membrane separation,<sup>5</sup> chemical sensing,<sup>6</sup> bioimaging,<sup>7,8</sup> and light-emitting diodes (LEDs),<sup>8–15</sup> mainly due to their advantages of high stability, easy synthesis, low cost, high photoelectric conversion capability, earth-abundance and low toxicity.<sup>1–10</sup>

As for their applications in LEDs,  $g\text{-C}_3\text{N}_4$ -based materials are mainly used as down-conversion luminescent materials (*i.e.*, phosphors) for replacing the currently widely-used, rare and expensive rare-earth-based ones (such as  $\text{Y}_3\text{Al}_5\text{O}_{12}\text{:Ce}^{3+}$ ,  $\text{SrAl}_4\text{-O}_7\text{:Eu}^{2+}, \text{Dy}^{3+}$ ,  $\text{Tb}_3\text{Al}_5\text{O}_{12}\text{:Ce}^{3+}$ ).<sup>8–15</sup> However, bulk  $g\text{-C}_3\text{N}_4$  just emits deep blue light, and its photoluminescence quantum yield (PLQY) is usually around 5.0%,<sup>11,14</sup> so it has very limited applications in LEDs. Therefore, the PLQY and colour need to be improved. Some strategies have been employed to achieve this goal, mainly including molecular doping,<sup>12–15</sup> atomic doping,<sup>8–10</sup> nanosizing,<sup>7,10,11</sup> and compositing.<sup>11</sup> Among them, molecular doping is a more promising method that can achieve better results. Moreover, many molecules with highly luminescent and stable organic groups can be utilized. Fluoranthene

(FA) should also be such a prospective group, because it is commonly used to construct various highly luminescent organic compounds.<sup>16–18</sup> Here, a  $g\text{-C}_3\text{N}_4$  derivative ( $g\text{-C}_3\text{N}_4\text{-PFA}$ ) modified by 3-phenylfluoranthene (PFA) groups was synthesized.  $g\text{-C}_3\text{N}_4\text{-PFA}$  had high luminescent efficiency and thermal stability, and was successfully used as a greenish-yellow metal-free phosphor in white LEDs (WLEDs).

As shown in Scheme 1,  $g\text{-C}_3\text{N}_4\text{-PFA}$  was synthesized *via* thermal polymerization. As described in ESI,† 6-(4-(fluoranthen-3-yl)phenyl)-1,3,5-triazine-2,4-diamine (FAPTD) was used as a molecular dopant and melamine was used as the main precursor. The preparation conditions were optimized by comparing the photoluminescence (PL) emission intensities of the samples obtained at different conditions. The higher the intensities, the better the corresponding conditions. As a result, the optimal conditions were a molar ratio of melamine to FAPTD of 15 : 1 and heating at 450 °C for 2 h (see the ESI† for details).

The  $g\text{-C}_3\text{N}_4\text{-PFA}$  sample obtained at the optimal conditions was characterized. As shown in Fig. 1(a), there were two strong peaks at 165.8 ppm and 157.0 ppm on the <sup>13</sup>C SSNMR spectrum,


 Scheme 1 Preparation route to  $g\text{-C}_3\text{N}_4\text{-PFA}$ .

Key Laboratory of Green-Chemistry Materials in University of Yunnan Province, National and Local Joint Engineering Research Center for Green Preparation Technology of Biobased Materials, School of Chemistry & Environment, Yunnan Minzu University, Kunming 650500, P. R. China. E-mail: tanghuaijun@sohu.com; yibingwu@ymu.edu.cn

 † Electronic supplementary information (ESI) available. See DOI: <https://doi.org/10.1039/d5ra02050f>

‡ These authors contributed equally to this work.



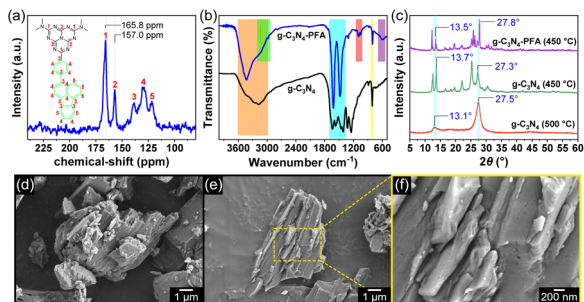


Fig. 1 (a)  $^{13}\text{C}$  SSNMR spectrum of  $\text{g-C}_3\text{N}_4\text{-PFA}$ . Inset: A representative structure unit of  $\text{g-C}_3\text{N}_4\text{-PFA}$ . (b) FTIR spectra of  $\text{g-C}_3\text{N}_4$  and  $\text{g-C}_3\text{N}_4\text{-PFA}$ . (c) Powder XRD patterns of  $\text{g-C}_3\text{N}_4$  and  $\text{g-C}_3\text{N}_4\text{-PFA}$ . (d)–(f) SEM images of  $\text{g-C}_3\text{N}_4\text{-PFA}$ .

which corresponded to C atoms (labelled as No. 1 and 2) of heptazine units.<sup>13–15</sup> The  $^{13}\text{C}$  signals of 3-phenylfluoranthene formed three peaks around 138.5 ppm (No. 3), 130.0 ppm (No. 4) and 122.0 ppm (No. 5). Both the FTIR spectra of  $\text{g-C}_3\text{N}_4$  and  $\text{g-C}_3\text{N}_4\text{-PFA}$  (Fig. 1(b)) showed typical breathing mode of heptazines at  $803\text{ cm}^{-1}$  and N–H stretching of  $\text{-NH}_2$  and  $\text{>NH}$  mainly at  $3000\text{--}3600\text{ cm}^{-1}$ .<sup>8,12–15</sup> Both of them showed C–N/C=N stretching of heptazines mainly at  $1350\text{--}1700\text{ cm}^{-1}$ ,<sup>8,12–15</sup> but the absorption of  $\text{g-C}_3\text{N}_4\text{-PFA}$  at here was stronger and merged into two peaks, due to the skeleton vibration absorption of the benzene rings overlapping at here. In addition to above commonalities of  $\text{g-C}_3\text{N}_4$  and  $\text{g-C}_3\text{N}_4\text{-PFA}$ , the stretching ( $2930\text{--}3200\text{ cm}^{-1}$ ), as well as the in-plane bending ( $1000\text{--}1150\text{ cm}^{-1}$ ) and out-of-plane bending ( $550\text{--}680\text{ cm}^{-1}$ ) vibration absorption peaks of C–H on benzene rings can be additionally observed in FTIR spectrum of  $\text{g-C}_3\text{N}_4\text{-PFA}$ . On the powder XRD pattern of  $\text{g-C}_3\text{N}_4$  synthesized at  $500\text{ }^\circ\text{C}$  (Fig. 1(c)), two characteristic peaks at  $13.1^\circ$  and  $27.5^\circ$  were observed, the former originated from the in-plane structural packing of the heptazines, the latter originated from the interplanar graphitic stacking.<sup>2,12–15</sup> Two such peaks (at  $13.5^\circ$  and  $27.8^\circ$ ) were also found in that of  $\text{g-C}_3\text{N}_4\text{-PFA}$ , which suggested  $\text{g-C}_3\text{N}_4\text{-PFA}$  was also composed of stacked heptazine-based 2D sheets. However, there were some additional sharp peaks due to its lower synthesis temperature (at  $450\text{ }^\circ\text{C}$ ) and PFA groups at the edge, resulting in lower polymerization degree, smaller 2D sheets and higher crystallinity.<sup>19</sup> Most of these peaks also appeared in the XRD pattern of  $\text{g-C}_3\text{N}_4$  synthesized at  $450\text{ }^\circ\text{C}$ , but they were more merged and broader, which suggested that PFA groups played a role in hindering high polymerization. The SEM images of  $\text{g-C}_3\text{N}_4\text{-PFA}$  (Fig. 1(d)–(f)) presented a layered stacked structure as many reported  $\text{g-C}_3\text{N}_4$ -based materials,<sup>12–15</sup> which was also consistent with its XRD results. At a higher magnification (Fig. 1(f)), some pores caused by  $\text{NH}_3$  generated during the polymerization can be seen. All the above results indicated that 2D layered  $\text{g-C}_3\text{N}_4\text{-PFA}$  had been successfully synthesized.

As shown in Fig. 2(a), relative to PL excitation (Ex) and emission (Em) spectra of  $\text{g-C}_3\text{N}_4$ , those of  $\text{g-C}_3\text{N}_4\text{-PFA}$  both showed obvious red shifts. The maximum Ex wavelength ( $\lambda_{\text{ex,max}}$ ) changed from  $375\text{ nm}$  to  $399\text{ nm}$ . The maximum Em wavelength ( $\lambda_{\text{em,max}}$ ) changed from  $468\text{ nm}$  to  $550\text{ nm}$ . To

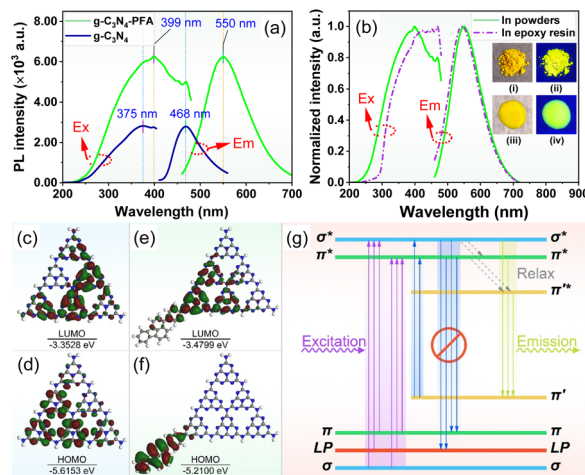


Fig. 2 (a) PL Ex and Em spectra of  $\text{g-C}_3\text{N}_4$  and  $\text{g-C}_3\text{N}_4\text{-PFA}$ . (b) PL Ex and Em spectra of  $\text{g-C}_3\text{N}_4\text{-PFA}$  in powders and epoxy resin (2.0 wt%). Inset: photographs of  $\text{g-C}_3\text{N}_4\text{-PFA}$  in powders under (i) natural light and (ii)  $450\text{ nm}$  blue light.  $\text{g-C}_3\text{N}_4\text{-PFA}$  in epoxy resin under (iii) natural light and (iv)  $450\text{ nm}$  blue light. (c)–(f) Electron density distribution and energy values of the LUMOs and HOMOs of  $\text{g-C}_3\text{N}_4$  model (c and d) and  $\text{g-C}_3\text{N}_4\text{-PFA}$  model (e and f). (g) Schematic energy levels diagram of radiative transition in  $\text{g-C}_3\text{N}_4\text{-PFA}$ .

understand how PFA groups affect PL properties, the electron density distributions and energy values of HOMOs and LUMOs of  $\text{g-C}_3\text{N}_4$  and  $\text{g-C}_3\text{N}_4\text{-PFA}$  models were calculated by density functional theory (DFT) in the Gaussian 16 suite of programs. As shown in Fig. 2(c)–(f), the electron density distributions of LUMO and HOMO were both on heptazine units in  $\text{g-C}_3\text{N}_4$ . The electron density distribution of LUMO remained on heptazine units in  $\text{g-C}_3\text{N}_4\text{-PFA}$  (but being different), while that of HOMO was on PFA. This indicated that PFA was an electron-donating group. As a result, bipolar structural units composed of PFA and heptazine were formed in  $\text{g-C}_3\text{N}_4\text{-PFA}$ . Generally, such separation of HOMO and LUMO and the resulting bipolar units is favourable to enhance luminescence efficiency.<sup>20,21</sup> Compared with the energy values of the LUMO ( $-3.3528\text{ eV}$ ) and HOMO ( $-5.6153\text{ eV}$ ) of  $\text{g-C}_3\text{N}_4$ , the energy value of LUMO of  $\text{g-C}_3\text{N}_4\text{-PFA}$  dropped to  $-3.4799\text{ eV}$ , but that of its HOMO rose to  $-5.2100\text{ eV}$ . Therefore, the energy gap ( $E_g$ ) decreased from  $2.2625\text{ eV}$  of  $\text{g-C}_3\text{N}_4$  to  $1.7301\text{ eV}$  of  $\text{g-C}_3\text{N}_4\text{-PFA}$ , which meant its emission would show an obvious red shift relative to that of  $\text{g-C}_3\text{N}_4$ . The ultraviolet-visible-near infrared diffuse reflectance spectra (UV-Vis-NIR DRS) and corresponding Tauc plots (Fig. S6 in ESI†) also revealed similar differences between  $\text{g-C}_3\text{N}_4$  and  $\text{g-C}_3\text{N}_4\text{-PFA}$ . The absorbance threshold of  $\text{g-C}_3\text{N}_4$  was  $450\text{ nm}$  (correspondingly,  $E_g = 2.76\text{ eV}$ ), that of  $\text{g-C}_3\text{N}_4\text{-PFA}$  redshifted to  $550\text{ nm}$  (correspondingly,  $E_g = 2.25\text{ eV}$ ).

In  $\text{g-C}_3\text{N}_4$ , electron transition of PL excitation and emission mainly happened between valence band (VB, including  $\sigma$ ,  $\pi$ , LP orbitals, LP: the lone pairs in 2p orbitals of the edge N atoms) and conduction band (CB, including  $\sigma^*$  and  $\pi^*$  orbitals).<sup>8,12,13</sup> Due to the grafting of PFA on heptazine units in  $\text{g-C}_3\text{N}_4\text{-PFA}$ , as shown in Fig. 2(g), the additional  $\pi'$  orbital (corresponding to its HOMO) and  $\pi'^*$  orbital (corresponding to its LUMO)



provided new pathways for electron transitions during PL excitation and emission (such as  $\sigma^* \rightarrow \pi'$ ,  $\pi^* \rightarrow \pi'$ ) with narrower  $E_g$ . Therefore, electrons in higher-energy orbitals  $\sigma^*$ ,  $\pi^*$  can relax to the lower-energy  $\pi^*$  orbital, which can promote  $\pi$  electron delocalization and reduce the non-radiative recombination of photogenerated electrons and holes.<sup>9,22</sup> As a result, the PL emission of g-C<sub>3</sub>N<sub>4</sub>-PFA not only exhibited a red shift but also showed an increase in luminescent efficiency. As for bulk g-C<sub>3</sub>N<sub>4</sub>, its PLQY is usually around 5.0%.<sup>11,14</sup> In this work, it was 4.4%, while that of g-C<sub>3</sub>N<sub>4</sub>-PFA was significantly increased to 36.7% (Fig. S7 in ESI†). This PLQY is still much lower than that of common commercial phosphors (such as ~75% of Y<sub>3</sub>Al<sub>5</sub>O<sub>12</sub>:Ce<sup>3+</sup>).<sup>23</sup> Nevertheless, it is higher than many reported g-C<sub>3</sub>N<sub>4</sub>-based luminescent materials, such as 5.4%,<sup>12</sup> 24.0%,<sup>13</sup> 11.3%,<sup>14</sup> and 27.09%<sup>15</sup> in literature, and it is a medium-level value.<sup>9,10</sup>

Since g-C<sub>3</sub>N<sub>4</sub>-PFA was doped in epoxy resin when it was used in LEDs, the PL excitation and emission spectra of g-C<sub>3</sub>N<sub>4</sub>-PFA in epoxy resin (2.0 wt%) were also measured. As shown in Fig. 2(b), compared with g-C<sub>3</sub>N<sub>4</sub>-PFA in powders, the stacking and aggregating degree of g-C<sub>3</sub>N<sub>4</sub>-PFA in epoxy resin may have decreased due to its dispersion. As a result, the PL emission showed a slight blue shift, the  $\lambda_{em,max}$  changed from 550 nm to 543 nm. The excitation spectrum of g-C<sub>3</sub>N<sub>4</sub>-PFA in epoxy resin showed a redshift (about 35 nm), probably due to the fact that the epoxy resin additionally provided a more polar environment.<sup>24,25</sup> Despite these differences, both g-C<sub>3</sub>N<sub>4</sub>-PFA in powders and in epoxy resin emitted greenish-yellow light (mainly at 450–700 nm), and the excitation spectra were both mainly at 300–500 nm, which meant it can be well excited by ultraviolet and blue light LED chips. The average lifetime of g-C<sub>3</sub>N<sub>4</sub>-PFA powders obtained from the triexponential fitting of its solid-state PL decay curve was 236.5 ns (Fig. S8 in ESI†), such a nanosecond level lifetime suggested it was suitable for LEDs.

As shown in Fig. 3(a), from 30 °C to 491 °C, the TG and DTG curves showed that g-C<sub>3</sub>N<sub>4</sub>-PFA just lost a small mass (5.0%) of adsorbed substances. Then the mass loss became more significant, which was caused by the thermal decomposition of the PFA groups and further thermal polymerization of g-C<sub>3</sub>N<sub>4</sub>-PFA, since the thermal decomposition of heptazine units usually happens around 600 °C (589 °C in this work).<sup>1,2</sup> Therefore, 491 °C can be considered as the thermal decomposition temperature ( $T_d$ ) of g-C<sub>3</sub>N<sub>4</sub>-PFA, which demonstrated high thermal stability and was enough to meet the heat-resistance requirements for LEDs ( $T_d > 150$  °C).<sup>13–15</sup> Temperature-dependent PL emission

spectra in Fig. 3(b) and (c) (the data of the spectra are listed in Table S1†) can demonstrate the thermal quenching property of g-C<sub>3</sub>N<sub>4</sub>-PFA. The range, shape and  $\lambda_{ex,max}$  of the spectra hardly changed, which suggested that the light-emitting colour was very stable and hardly changed with the change of temperature. Relative to the intensity at 30 °C, that at 90 °C was 91.7% and that at 150 °C was 74.1%, which suggested that g-C<sub>3</sub>N<sub>4</sub>-PFA had a low level of thermal quenching. The thermal quenching was not only lower than that of some reported g-C<sub>3</sub>N<sub>4</sub> derivatives,<sup>14,26</sup> but also lower than that of many reported inorganic phosphors.<sup>23,27–30</sup> Moreover, as the temperature dropped, the intensities can gradually recover. The thermal stability and thermal quenching property suggested that g-C<sub>3</sub>N<sub>4</sub>-PFA was suitable for being used in LEDs.

Two kinds of LEDs were fabricated. (i) only g-C<sub>3</sub>N<sub>4</sub>-PFA was used as phosphors (LEDs No. 1–8, the performance data were listed in Table S2 in ESI†); (ii) g-C<sub>3</sub>N<sub>4</sub>-PFA together with rare-earth-free red-emitting K<sub>2</sub>SiF<sub>6</sub>:Mn<sup>4+</sup> as phosphors (LEDs No. 9–15, the performance data were listed in Table 1). All the LEDs were excited by GaN-based blue light chips (460 nm, 25 lm W<sup>-1</sup>) and tested under 3.0 V and 20 mA.

When only g-C<sub>3</sub>N<sub>4</sub>-PFA was used as phosphors, its blending concentrations in epoxy resin increased from 1.0 wt% to 8.0 wt%. During this process, as shown in Fig. 4(a), the blue light of the chips gradually weakened, while the greenish-yellow light of g-C<sub>3</sub>N<sub>4</sub>-PFA gradually became stronger. Finally, at 8.0 wt%, the blue light was completely absorbed by g-C<sub>3</sub>N<sub>4</sub>-PFA and disappeared, and the greenish-yellow light (CIE: 0.46, 0.51) of the LED originated from only g-C<sub>3</sub>N<sub>4</sub>-PFA. Although three WLEDs (No. 2–4) were obtained when only g-C<sub>3</sub>N<sub>4</sub>-PFA was used as phosphors, due to the lack of red-light component, their correlated colour temperatures (CCTs) were high, and the colour rendering indexes (CRIs) were low, which was very similar to the situation of the widely-used Y<sub>3</sub>Al<sub>5</sub>O<sub>12</sub>:Ce<sup>3+</sup>-based WLEDs, and their applications will be limited.<sup>23,29</sup>

Based on LED No. 2, when red-emitting K<sub>2</sub>SiF<sub>6</sub>:Mn<sup>4+</sup> was added in, a series of new WLEDs (No. 9–15) were obtained. As listed in Table 1, in comparison with the data of LED No. 2, the CRIs were obviously improved. The CRIs of LEDs No. 9–12 were higher than 80. Especially, the CRIs of No. 10 (85.4) and No. 11 (87.0) were higher than 85. The CCTs gradually decreased with the increase of the amount of K<sub>2</sub>SiF<sub>6</sub>:Mn<sup>4+</sup>. Except for LED No.

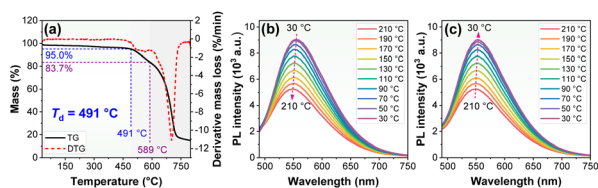


Fig. 3 (a) TG and DTG of g-C<sub>3</sub>N<sub>4</sub>-PFA powders. (b) and (c) Temperature-dependent PL spectra ( $\lambda_{ex} = 450$  nm) of g-C<sub>3</sub>N<sub>4</sub>-PFA powders ((b) from 30 °C to 210 °C, (c) from 210 °C to 30 °C, measured at every 20 °C interval).

Table 1 Performance data of LEDs No. 2, 9–15 (blending concentrations of g-C<sub>3</sub>N<sub>4</sub>-PFA were fixed at 2 wt%)

No. of LEDs	K <sub>2</sub> SiF <sub>6</sub> :Mn <sup>4+</sup> (wt%)	LE (lm W <sup>-1</sup> )	CRI	CCT (K)	CIE (x, y)
2	0.0	35.02	76.6	16 313	(0.26, 0.27)
9	1.0	46.70	81.6	13 320	(0.27, 0.27)
10	2.0	43.14	85.4	9681	(0.28, 0.29)
11	3.0	47.18	87.0	7753	(0.30, 0.30)
12	4.0	45.60	84.6	6771	(0.31, 0.31)
13	5.0	48.60	78.5	5927	(0.32, 0.31)
14	6.0	51.24	78.1	5066	(0.34, 0.32)
15	7.00	48.48	70.6	4191	(0.36, 0.32)



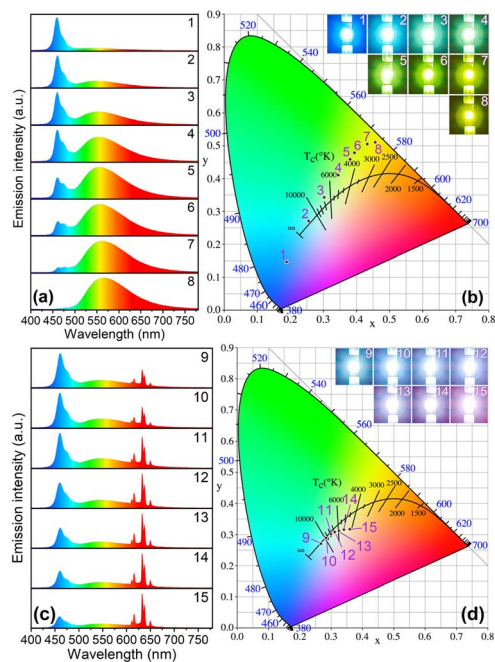


Fig. 4 (a) and (c) Emission spectra of LEDs No. 1–15. (b) and (d) CIE chromaticity coordinates of LEDs No. 1–15. Inset: Working state photographs of LEDs No. 1–15.

9, the CIE chromaticity coordinates of the other LEDs all were near (0.33, 0.33) of standard white light, which indicated most of them can emit good-quality white light.

In summary, a 3-phenylfluoranthene-modified greenish-yellow-emitting  $g\text{-C}_3\text{N}_4$  derivative ( $g\text{-C}_3\text{N}_4\text{-PFA}$ ) was successfully synthesized. Its PLQY was up to 36.7%,  $T_d$  was up to 491 °C, and thermal quenching was low. When used together with  $\text{K}_2\text{SiF}_6\text{:Mn}^{4+}$  as phosphors, under the excitation of 460 nm GaN-based blue light chips, a series of high-performance WLEDs with high CRIs and proper CCTs were prepared.

## Data availability

The data supporting this article have been included as part of the ESI.†

## Author contributions

Jinghao Zhang and Long Wang: conceptualization, data curation, investigation, methodology, writing-original draft. Huaijun Tang: conceptualization, data curation, funding acquisition, investigation, methodology, supervision, writing-original draft, writing-reviewing and editing. Xiang Li, Aijing Jiang, Shanglan Xian, Rongman Xia, Yifei Li and Zhouyang Jiang: data curation, investigation. Yibing Wu: data curation, investigation, methodology, project administration. Zhengliang Wang: supervision.

## Conflicts of interest

There are no conflicts to declare.

## Acknowledgements

The authors thank the projects of National Natural Science Foundation of China (No. 22361054, 21762049 and 21262046).

## Notes and references

- 1 Y. Tong, J. Xia, Y. Hu, Y. He, G. He and H. Chen, *Chem. Commun.*, 2025, **61**, 1509–1532.
- 2 W.-J. Ong, L.-L. Tan, Y. H. Ng, S.-T. Yong and S.-P. Chai, *Chem. Rev.*, 2016, **116**, 7159–7329.
- 3 F. K. Kessler, Y. Zheng, D. Schwarz, C. Merschjann, W. Schnick, X. Wang and M. J. Bojdys, *Nat. Rev. Mater.*, 2017, **2**, 17030.
- 4 Y. Luo, Y. Yan, S. Zheng, H. Xue and H. Pang, *J. Mater. Chem. A*, 2019, **7**, 901–924.
- 5 Y. Wang, N. Wu, Y. Wang, H. Ma, J. Zhang, L. Xu, M. K. Albolqany and B. Liu, *Nat. Commun.*, 2019, **10**, 2500.
- 6 J. Tian, Q. Liu, A. M. Asiri, A. O. Al-Youbi and X. Sun, *Anal. Chem.*, 2013, **85**, 5595–5599.
- 7 X. Zhang, H. Wang, H. Wang, Q. Zhang, J. Xie, Y. Tian, J. Wang and Y. Xie, *Adv. Mater.*, 2014, **26**, 4438–4443.
- 8 H. Zhang, D. Zheng, Z. Cai, Z. Song, Y. Xu, R. Chen, C. Lin and L. Guo, *ACS Appl. Nano Mater.*, 2020, **3**, 6798–6805.
- 9 Y. Wang, M. Zhang, L. Wang and J. Xing, *Adv. Opt. Mater.*, 2023, **11**, 2301547.
- 10 H. Y. Hoh, Y. Zhang, Y. L. Zhong and Q. Bao, *Adv. Opt. Mater.*, 2021, **9**, 2100146.
- 11 W. Liu, S. Xu, S. Guan, R. Liang, M. Wei, D. G. Evans and X. Duan, *Adv. Mater.*, 2018, **30**, 1704376.
- 12 Q. Guo, M. Wei, Z. Zheng, X. Huang, X. Song, S.-B. Qiu, X.-b. Yang, X. Liu, J. Qiu and G. Dong, *Adv. Opt. Mater.*, 2019, **7**, 1900775.
- 13 H. Tang, Q. Chen, G. Meng, S. Lu, J. Qin, K. Yang, L. Gao, Z. Wang and Y. He, *RSC Adv.*, 2023, **13**, 12509.
- 14 H. Tang, Q. Chen, S. Lu, X. Li, H. Li, Y. Wang, K. Wang, Q. Zhou and Z. Wang, *J. Lumin.*, 2022, **244**, 118734.
- 15 Z. Huang, H. Xu, Y. Luo, R. Zhang and Y. Wang, *Appl. Surf. Sci.*, 2025, **685**, 162054.
- 16 Y.-H. Lee, T.-C. Wu, C.-W. Liaw, T.-C. Wen, T.-F. Guo and Y.-T. Wu, *J. Mater. Chem.*, 2012, **22**, 11032.
- 17 X. Sun, M.-Y. Liao, X. Yu, Y.-S. Wu, C. Zhong, C.-C. Chueh, Z. Li and Z. Li, *Chem. Sci.*, 2022, **13**, 996.
- 18 X.-G. Li, Y. Liao, M.-R. Huang, V. Strong and R. B. Kaner, *Chem. Sci.*, 2013, **4**, 1970.
- 19 V. W. Lau, M. B. Mesch, V. Duppel, V. Blum, J. Senker and B. V. Lotsch, *J. Am. Chem. Soc.*, 2015, **137**, 1064–1072.
- 20 J. Liu, S. Wang, W. Lv, J. Wu, Q. Ling and Z. Lin, *Adv. Funct. Mater.*, 2024, **34**, 2402578.
- 21 Y. Sun, H. Wang, S. Liu, X. Lu, Z. Feng, D. Zhong, D. Jia, X. Yang, B. Su, Y. Sun, B. Jiao and G. Zhou, *Innovation Mater.*, 2023, **1**, 100028.
- 22 Q. Cui, J. Xu, X. Wang, L. Li, M. Antonietti and M. Shalom, *Angew. Chem., Int. Ed.*, 2016, **55**, 3672–3676.
- 23 S. Ye, F. Xiao, Y. X. Pan, Y. Y. Ma and Q. Y. Zhang, *Mater. Sci. Eng., R*, 2010, **71**, 1–34.



## Paper

- 24 P. M. Gharat, S. Muralidharan, M. Sundararajan, H. Pal and S. D. Choudhury, *ChemistrySelect*, 2017, **2**, 9751–9759.
- 25 S. Yan, Z. Lü, Z. Chen, X. Wang and J. Xiao, *J. Lumin.*, 2025, **280**, 121110.
- 26 S. Lu, H. Tang, J. Qin, L. Gao, W. Li, K. Yang, Y. Jiao, S. Xian, L. Wang, Q. Zhou and Z. Wang, *Opt. Mater.*, 2023, **142**, 114076.
- 27 Q. Shao, H. Lin, Y. Dong and J. Jiang, *J. Lumin.*, 2014, **151**, 165–169.
- 28 W. B. Im, N. N. Fellows, S. P. DenBaars and R. Seshadri, *J. Mater. Chem.*, 2009, **19**, 1325–1330.
- 29 H. Li, R. Zhao, Y. Jia, W. Sun, J. Fu, L. Jiang, S. Zhang, R. Pang and C. Li, *ACS Appl. Mater. Interfaces*, 2014, **6**, 3163–3169.
- 30 A. A. Setlur, R. J. Lyons, J. E. Murphy, N. P. Kumar and M. S. Kishore, *ECS J. Solid State Sci. Technol.*, 2013, **2**, R3059–R3070.

